Supporting Information

Persson and Halle 10.1073/pnas.0709585105

SI Text

Preparation of Cell Samples. Cultures were grown in LB medium (5 g liter^{-1} yeast extract, 10 g liter^{-1} tryptone, 10 g liter^{-1} NaCl) for *E. coli* and in DSMZ's Halobacteria Medium 372 (5 g liter^{-1} yeast extract, 5 g liter^{-1} casamino acids, 1 g liter^{-1} sodium glutamate, 2 g liter^{-1} KCl, 3 g liter^{-1} sodium citrate, 20 g liter^{-1} $MgSO_4{\cdot}7H_2O$, 200 g liter^{-1} NaCl, 36 mg liter^{-1} $FeCl_2{\cdot}4H_2O$, 0.36 mg liter^{-1} $MnCl_2{\cdot}4H_2O$, pH* 7.1) for *H. marismortui*. The H_2O media were autoclaved and the D_2O media were sterile filtered through 0.45-μm filters (Sartorius).

After rehydration, the bacteria were grown on agar plates prepared with growth medium (in H_2O) and incubated at 37°C. *H. marismortui* formed bright red colonies. 50-ml aliquots of growth medium (in H_2O) were inoculated with individual colonies and incubated in baffled flasks at 37°C under shaking at 120 rpm. At $OD_{600} \approx 1$, 0.5 ml of each culture was used to inoculate 50 ml deuterated medium and incubated under the same conditions until $OD_{600} \approx 1$. 6.5 ml of each culture was then used to inoculate 3 × 500 ml of freshly prepared deuterated medium in 2.5-liter baffled flasks and incubated at 37°C under shaking. *E. coli* grew to an OD_{600} of 1.0 – 1.3 in 6 h with a generation time of 50 min and *H. marismortui* grew to an OD_{600} of 0.6 – 0.8 in 24 h with a final generation time of 7.7 h. The cultures were harvested by centrifugation for 25 min at 5,000 × *g* and washed twice with 150 ml D_2O-saline containing 8.8 g liter^{-1} NaCl, 0.37 g liter^{-1} KCl and 10 mM Tris·HCl at pD 8.0 for *E. coli* and 200 g liter^{-1} NaCl, 95.5 g liter^{-1} $MgSO_4{\cdot}7H_2O$, 0.66 g liter^{-1} $CaCl_2{\cdot}2H_2O$, 2 g liter^{-1} KCl and 10 mM Tris·HCl at pD 8.0 for *H. marismortui*. A final centrifugation was performed for 30 min at 10,000 ×*g* to obtain a densely packed cell mass. A portion of this cell mass was centrifuged down into a 10-mm NMR tube, while another portion was heated to 130°C for 12 h to determine the water content of the sample: 3.48 g D_2O (g DCM)$^{-1}$ for *E. coli* and 1.52 g D_2O (g DCM)$^{-1}$ for *H. marismortui* (Table 1). These water contents agree closely with values reported for similarly prepared samples of *E. coli* (1–3) and *H. marismortui* (1). Samples for ^{1}H MRD were prepared in the same way, except that culture media and washing solutions (pH 7.6) were made from H_2O rather than D_2O.

Characterization of Cell Samples. The intracellular water content depends on the external osmolality. At 0.40 osM kg^{-1}, as for our *E. coli* sample, the water-accessible intracellular volume is 2.33 ml (g DCM)$^{-1}$ (2). The fraction intracellular water in our *E. coli* sample is therefore $f_{cell} = (2.33/3.48) \times (20.02/18.02) = 0.744$. Water occupies 70% of the cell volume (3), so the extracellular volume fraction of the sample is $0.256/(0.256 + 0.744/0.70) = 0.194$. For a sample of *H. marismortui* prepared in a similar way as here, an extracellular volume fraction of 0.211 was reported (4), close to that of our *E. coli* sample. Therefore, also f_{cell} should be similar for the two samples. (The *H. marismortui* sample has a high salt content, but the intracellular and extracellular salt concentrations are similar so f_{cell} is hardly affected.)

The chemical composition of the *E. coli* cell depends on growth rate, but is nearly independent of culture medium and temperature (3, 5). At our growth rate, the protein mass fraction is 572 mg (g DCM)$^{-1}$ (5). During MRD measurements, the cells were in stationary phase, deprived of nutrients and oxygen. Although the transition from balanced growth to stationary phase is accompanied by morphological and chemical changes (6), the total protein mass changes little during the first several hours of starvation (7).

The elemental composition of 1 g of dry cell mass (DCM) from each our samples was analyzed by inductively coupled plasma sector field mass spectrometry (performed at ALS Analytica, Luleå, Sweden). The results are shown in Table S2. The nitrogen mass fraction, 140 mg (g DCM)$^{-1}$, for the *E. coli* sample is in the expected range (8). Complete amino analysis (performed at the Amino Acid Analysis Center, Dept. of Biochemistry and Organic Chemistry, Uppsala University, Sweden) on the *H. marismortui* sample (after MRD measurements) yielded a total protein mass fraction of 356 mg (g DCM)$^{-1}$. The water/protein mass ratio (Table 1) obtained by combining this value with the water mass fraction in the sample (see above), is within 2% of the value reported for a similar sample (4).

Cell Viability Control. To assess the extent of cell death during the 6 h MRD measurement period, an *E. coli* sample was prepared as described above, except that also the washing saline was sterile filtered. Before the final centrifugation at 10,000 ×*g*, 0.5 ml of the 20-ml cell suspension was removed and diluted in 23 ml H_2O-saline buffer to a concentration of 2.9 mg cells ml^{-1} (determined by weighing the cell pellet after the final centrifugation). The suspension was gently mixed and 1 ml was aseptically transferred to 99 ml of H_2O-saline. This dilution step was repeated three more times to produce dilutions of 10^{-4}, 10^{-6}, and 10^{-8}. The two most dilute suspensions were plated on 3 × 5 agar plates with LB medium and colonies were counted after incubation at 37°C overnight. The original cell pellet was maintained at 27°C for 6 h following the final centrifugation, whereupon a portion of the cell mass was resuspended in H_2O-saline to a concentration of 3.0 mg cells ml^{-1}. Serial dilution, plating, and colony counting were then performed as described above. Averaging over plates with 30–300 colonies, the concentration of viable cells was determined to $(3.4 \pm 0.3) \times 10^9$ cells ml^{-1} before and $(2.4 \pm 0.1) \times 10^9$ cells ml^{-1} after the 6-h period at 27°C. From these results, we conclude that 70 ± 7% of the cells survived the full duration of the MRD experiments.

Fast-Exchange Approximation. The high-frequency relaxation rate $R_1(\omega_0^*)$ is analyzed under the assumption of fast water exchange between the intracellular and extracellular compartments so that

$$R_1(\omega_0^*) = f_{cell} R_{1,cell}(\omega_0^*) + (1 - f_{cell}) R_{1,ext}(\omega_0^*) \qquad [1]$$

This relation is valid provided that

$$\tau_{cell} \ll \frac{1}{(1 - f_{cell})|R_{1,cell}(\omega_0^*) - R_{1,ext}(\omega_0^*)|} \qquad [2]$$

where τ_{cell} is the mean residence time of a water molecule in the cell. For the *E. coli* sample, $R_1(\omega_0^*) = 5.38\ s^{-1}$, $R_1^0 = 2.15\ s^{-1}$ and $f_{cell} = 0.744$ (see above). With $R_{1,ext}(\omega_0^*) = R_1^0$ (since there are virtually no dissolved macromolecules outside the cell), Eqs. **1** and **2** yield the fast-exchange condition $\tau_{cell} \ll 0.9$ s. For a spherical cell of radius R_{cell} with intracellular water volume fraction ϕ_W, the residence time is related to the (diffusive) permeability P of the cell membrane as

$$\tau_{cell} = \frac{\phi_W R_{cell}}{3P} \qquad [3]$$

The outer membrane of *E. coli* is highly permeable to water and polar solutes up to ≈600 Da (9), so P is the permeability of the cytoplasmic membrane. Three (passive) mechanisms contribute

to P (10, 11): (*i*) the intrinsic water permeability of the phospholipid bilayer, (*ii*) water transport via the *E. coli* aquaporin (AqpZ) and aquaglyceroporin (GlpF), and (*iii*) cotransport of water via ion, glucose and other channels. The intrinsic water permeability of a planar bilayer membrane made from *E. coli* lipid extract is 40 μm s^{-1} at 27°C (12). If this were the only mechanism of water permeation, we would have for our *E. coli* cells, with $\phi_W = 0.7$ and $R_{cell} = 1$ μm for the nearly spherical (6) starving cells, $\tau_{cell} = 0.7 \times 1 / (3 \times 40)$ s = 6 ms. With the additional permeability contributed by aquaporins (13), τ_{cell} may be as short as 1–2 ms. But the fast-exchange condition is satisfied with a wide margin even without taking aquaporins into account, and this should be the case also for *H. marismortui*.

Labile-Deuteron Exchange. For the nutrient starved and anoxic cells in our MRD samples, the intracellular pD equals the extracellular (buffered) pD of 8.0 (14–16). At this pD, exchange of labile deuterons occurs mainly by the OD-catalyzed mechanism and the mean residence time, τ_L, of a labile deuteron of type L is given by (17)

$$\frac{1}{\tau_L} = k_2^L 10^{pD - pK_W^D} + k_3^L(pD) \qquad [4]$$

where the second term accounts for other exchange catalysts than D_3O^+ and OD^-, such as phosphate ions or biomolecular groups. For D_2O at 27°C, $pK_W^D = 14.80$. At pD 8.0, virtually all carboxyl groups and His residues are deprotonated, whereas other labile groups are fully protonated. The classes of labile hydrogens that we need to consider are then O–D in hydroxyl groups (mainly Ser, Thr, and Tyr in proteins and hydroxyl groups in saccharides) and N–D in amino groups (mainly Lys in proteins and amino groups in A, G and C nucleotide bases), in imino groups (all nucleotide bases) and in guanidino groups (Arg in proteins). For all these labile deuterons, the rate constant k_2 (in D_2O at 27°C) is in the range 10^9–10^{10} M^{-1} s^{-1} (17–23). For simplicity, we adopt a common value, $k_2 = 5 \times 10^9$ M^{-1} s^{-1}. N–D deuterons in amide groups (Asn, Gln and peptide) and indole groups (Trp) exchange much more slowly and can be neglected. We also neglect S–D hydrogens (free Cys) and N–D in polyamines (which are strongly bound to DNA).

The main contributor to the second term in Eq. **4** is probably phosphate (inorganic and organic). For aerobically respiring *E. coli* cells in exponential or stationary phase, the combined amount of inorganic phosphate, ADP and ATP is ≈5 μmol (g DCM)$^{-1}$ (24), corresponding, at our water content, to an intracellular phosphate concentration of ≈2 mM. At this concentration, the effect of phosphate catalysis is negligible even in H_2O at pH 7 (18). Since the second term involves the product $[H_2PO_4^-][HPO_4^{2-}]$ and since $H_2PO_4^-$ has a pK_a value of 7.2, the effect should be even smaller at pD 8.0. We thus neglect the second term in Eq. **4**, which then yields $\tau_L = 1.3$ ms.

The Dynamic Perturbation Factor. The high-frequency excess relaxation quantity $\rho(\omega_0^*)$ can be formally decomposed into contributions from water molecules with correlation times shorter (α class) or longer (β class) than $\tau^* = 1/\omega_0^* = 2$ ns:

$$\rho(\omega_0^*) = f_\alpha \rho_\alpha(\omega_0^*) + f_\beta \rho_\beta(\omega_0^*) \qquad [5]$$

where f_α and $f_\beta = 1 - f_\alpha$ are the relative population of the two water classes and

$$\rho_\alpha(\omega_0^*) = \frac{\langle R_1^\alpha(\omega_0^*)\rangle}{R_1^0} - 1 \qquad [6a]$$

$$\rho_\beta(\omega_0^*) = \frac{\langle R_{1,\mathrm{eff}}^\beta(\omega_0^*)\rangle}{R_1^0} - 1 \qquad [6b]$$

We show first that the β contribution to $\rho(\omega_0^*)$ is negligibly small compared to the α contribution. At the high frequency ω_0^*, $\langle R_{1,\mathrm{eff}}^\beta(\omega_0^*)\rangle$ is dominated by hydration sites with correlation times, τ_β, not much longer than τ^*, that is, deep surface pockets and internal cavities in freely tumbling macromolecules. For such short correlation times, the conventional perturbation theory of spin relaxation (motional narrowing regime) (25) is valid and

$$\langle R_{1,\mathrm{eff}}^\beta(\omega_0^*)\rangle = \left\langle \frac{1}{\tau_{W,\beta} + 1/R_1^\beta(\omega_0^*)} \right\rangle \qquad [7]$$

where $\tau_{W,\beta}$ is the mean residence time of a water molecule in a particular β site. From Eqs. **5–7**, we obtain an upper bound for the β contribution to $\rho(\omega_0^*)$:

$$f_\beta \rho_\beta(\omega_0^*) < f_\beta \frac{\langle R_1^\beta(\omega_0^*)\rangle}{R_1^0} < \frac{f_\beta}{\tau_0}\left\langle \frac{0.2\tau_\beta}{1 + (\omega_0^*\tau_\beta)^2} + \frac{0.8\tau_\beta}{1 + (2\omega_0^*\tau_\beta)^2} \right\rangle \qquad [8]$$

where $\tau_0 R_1^0/\omega_Q^2 = 2.15 / (8.70 \times 10^5)^2 = 2.8$ ps is the bulk D_2O correlation time at 27°C. The first inequality in Eq. **8** comes from assuming fast exchange [$\tau_{W,\beta} R_1^\beta(\omega_0^*) \ll 1$] and neglecting the –1 term in Eq. **6b**. The second inequality comes from setting the order parameter in $R_1^\beta(\omega_0^*)$ to 1 (26). A conservative upper bound for the β class average in Eq. **8** is obtained by asserting that *all* β waters have the minimum correlation time, τ^*. Then Eq. **8** yields

$$f_\beta \rho_\beta(\omega_0^*) \ll \frac{13\ f_\beta}{50\omega_0^*\tau_0} = \frac{f_\beta}{5.3 \times 10^{-3}} \qquad [9]$$

where we have inserted $\omega_0^*/(2\pi) = 76.8$ MHz and $\tau_0 = 2.8$ ps. Our results (Table 1) indicate that $f_\beta < 5.3 \times 10^{-3}$, so we conclude that $f_\beta \rho_\beta \omega_0^* \ll 1$. Since $\rho(\omega_0^*) > 1$ (Table 1), the β contribution can thus be neglected.

We can now express Eqs. **5** and **6a** as

$$\rho(\omega_0^*) = f_\alpha[\xi_\alpha(\omega_0^*) - 1] \qquad [10]$$

where we have introduced the *apparent* dynamic perturbation factor (DPF) $\xi_\alpha(\omega_0^*)$, defined as

$$\xi_\alpha(\omega_0^*) \equiv \frac{\langle R_1^\alpha(\omega_0^*)\rangle}{R_1^0} \qquad [11]$$

We show next that the apparent DPF $\xi_\alpha(\omega_0^*)$ can, to a good approximation, be equated with the *true* DPF ξ_α^0, defined as the ratio of the mean correlation time $\langle\tau_\alpha\rangle$ for all hydration sites in class α to the correlation time τ_0 in bulk water:

$$\xi_\alpha^0 \equiv \frac{\langle\tau_\alpha\rangle}{\tau_0} \qquad [12]$$

The true DPF is thus a global measure of the relative slowing down of water dynamics in class α. Because the quadrupole frequency ω_Q cancels out in the ratio in Eq. **11**, the apparent DPF is given by

$$\xi_\alpha(\omega_0^*) = \frac{1}{\tau_0}\left\langle \frac{0.2\tau_\alpha}{1 + (\omega_0^*\tau_\alpha)^2} + \frac{0.8\tau_\alpha}{1 + (2\omega_0^*\tau_\alpha)^2} \right\rangle \qquad [13]$$

Clearly, $\xi_\alpha(0) = \xi_\alpha^0$. Class α contains water molecules with correlation times τ_α up to $\tau^* = 1/\omega_0^*$. The α dispersion has therefore not quite reached its low-frequency plateau at the

frequency ω_0^* and the apparent DPF $\xi_\alpha(\omega_0^*)$ is slightly smaller than the true DPF ξ_α^0.

To estimate the difference between the true and apparent DPFs, we must compute the α class average in Eq. **13**. To this end, we assume that the correlation time τ_α in class α has a power-law distribution, $f(\tau_\alpha) : \tau_\alpha^{-\gamma}$, normalized on the range $[\tau_0, \tau^*]$. We thus find that the ratio $\xi(\omega_0^*)/\xi_\alpha^0$ goes from [atan (1) + 2 atan (2)]/5 $\approx$ 0.600 for $\gamma = 1$ to 0.997 for $\gamma = 3$ (Fig. S1). Indeed, for large γ, the distribution places nearly all weight on the shortest correlation times, $\tau_\alpha \approx \tau_0$, so $(\omega_0\tau_\alpha)^2 \ll 1$ for nearly all α waters and Eq. **13** reduces to Eq. **12**. Based on MRD studies of protein solutions, we expect γ to be close to 2 (C. Mattea, J. Qvist, and B.H., unpublished work). The apparent DPF should thus be ≈10% smaller than the true DPF (Fig. S1). Disregarding this minor difference, we can obtain the true DPF as

$$\xi_\alpha^0 = 1 + \frac{\rho(\omega_0^*)}{f_\alpha} \qquad [14]$$

The error incurred by equating the apparent and true DPFs is partly cancelled by the neglect of the β contribution to $\rho(\omega_0^*)$, which leads us to overestimate $\xi_\alpha(\omega_0^*)$. The combined error introduced by these two approximations is not likely to exceed 10% of $\rho(\omega_0^*)$. In the main text, we have dropped the zero superscript on ξ_α^0, and the α class is either the intracellular water molecules with $\tau < \tau^*$ (ξ_{cell}) or the hydration water molecules with $\tau < \tau^*$ (ξ_{hyd}).

Neglect of Weakly Perturbing Solutes. The high-frequency excess relaxation quantity $\rho(\omega_0^*)$ is a population-weighted sum of contributions from hydration water in different classes of solutes, S:

$$\rho(\omega_0^*) = \sum_S f_S \rho_S(\omega_0^*) \qquad [15]$$

with $\rho(\omega_0^*)$ defined as in Eq. **6a**. The relative population f_S can be expressed as $\nu_S\, n_S/n_W$, where n_S/n_W is the solute/water mole ratio in the sample and ν_S is the (primary) hydration number of the solute S. We now show that the contributions to $\rho(\omega_0^*)$ from the hydration water of phospholipids, saccharides and small molecules and ions is negligibly small, leaving proteins and nucleic acids as the dominant cause of dynamic perturbation of hydration water. This is consistent with the finding that water molecules in geometrically secluded hydration sites, which are found only on macromolecular solutes, are much more motionally retarded than water molecules in contact with the fully exposed parts of the solute's surface (27).

The most abundant inorganic ions in the intracellular as well as the extracellular regions are Na^+ and K^+. The mole ratios n_{Na}/n_W and n_K/n_W for the two cell samples, obtained from elemental analysis (Table S2), imply that, if the Na^+ and K^+ ions have intact first hydration shells (with $\nu = 6$), 50% of the water molecules in the *H. marismortui* sample (but only 3% in the *E. coli* sample) are in direct contact with a Na^+ or K^+ ion. If also the counterions are taken into account (Cl^- is only abundant in *H. marismortui*), then an even larger fraction of the water molecules would be directly coordinated to ions.

The quantities $\nu_{Na}\rho_{Na}$ and $\nu_K\rho_K$ have been determined from water-^{2}H relaxation measurements on aqueous NaCl and KCl solutions at 25°C (28). While the effects of the cation and anion cannot be separated experimentally, it is generally assumed that the Cl^- counterion has a negligible effect on water relaxation (28). Therefore, it is not important to know the Cl^- concentration in our samples. Previous investigators have usually reported the quantity $B = \nu_S\, \rho_S\, /\, 55.5$. Thus, $B_{Na} = 0.05 \pm 0.01$ and $B_K = -0.027 \pm 0.003$ (28). Using these values and the mole ratios, we find that the combined contribution to $\rho(\omega_0^*)$ from Na^+ and K^+ ions is not significantly different from zero for the *E. coli* sample: $(6 \pm 13)\times10^{-4}$. For the *H. marismortui* sample, this contribution is two orders of magnitude larger, $(6 \pm 2)\times10^{-2}$, but still only 3% of $\rho(\omega_0^*)$. Note that, despite the high Na^+ and K^+ content of the *H. marismortui* sample, the *total* effect of these ions on water *dynamics* (and ^{2}H relaxation) is much smaller than the combined effect of other solutes. This is partly because of the opposite effects of Na^+ and K^+ ions. Presumably, the high salt content has more profound *thermodynamic* consequences.

The samples also contain multivalent ions, like Mg^{2+}, Ca^{2+} and $Fe^{2+/3+}$, and in substantially higher amounts in *H. marismortui* than in *E. coli* (Table S2). Nevertheless, these amounts are relatively small and virtually all of these multivalent ions are strongly bound to specific sites in proteins and nucleic acids. To the extent that water molecules are coordinated by these bound ions, they are best considered as contributing to the hydration water of the macromolecular host.

For *E. coli* under our growth conditions, metabolites, cofactors and ions account for 38.2 mg (g DCM)$^{-1}$ (3, 5). Most of this fraction comes from intracellular K^+ ions, which make a negligible contribution to $\rho(\omega_0^*)$ (see above). According to our elemental analysis (Table S2), the *E. coli* sample contains 24.2 mg K (g DCM)$^{-1}$, of which only 0.16 mg K (g DSM)$^{-1}$ is extracellular. Thus, there remains only 14 mg (g DCM)$^{-1}$ to account for. The most abundant free organic metabolite in *E. coli* is glutamate (29). Assuming that glutamate accounts for all of the 14 mg (g DCM)$^{-1}$, we have $n_{\text{glutamate}}/n_W = 5.5 \times 10^{-4}$. The quantity $\nu_S\, \rho_S$ is only available for a few amino acids (30), but a reasonable estimate is, $\nu_{\text{glutamate}}\, \rho_{\text{glutamate}} \approx 10$. We thus obtain $f_{\text{glutamate}}\rho_{\text{glutamate}} \approx 0.005$, which is merely 0.36% of $\rho(\omega_0^*)$. Cofactors at still lower concentration would also make a negligible contribution if they were freely dissolved in the cytoplasm, but they are actually strongly bound to macromolecules and thus contribute even less.

E. coli contains glucosidic or related residues in several cellular components (3, 5): 168 μmol (g DCM)$^{-1}$ in glycogen, 60 μmol (g DCM)$^{-1}$ in peptidoglycan (murein in the cell wall on the inside of the outer membrane), and 73 μmol (g DCM)$^{-1}$ in lipopolysaccharides (on the outside of the outer membrane). If these sugar residues are fully solvent-exposed, we have $n_{\text{glucose}} = 301$ μmol (g DCM)$^{-1}$, $\nu_{\text{glucose}}\, \rho_{\text{glucose}} = 15$ (this is an upper estimate for a glucose residue in a longer oligosaccharide (31)), and $f_{\text{glucose}}\rho_{\text{glucose}} = 0.026$, or 1.7% of $\rho(\omega_0^*)$. The peptidoglycan component also contains 120 μmol (g DCM)$^{-1}$ amino acid-like residues (3), which (see above) contribute less than 0.0069 (0.46%) to $\rho(\omega_0^*)$.

E. coli contains $n_{\text{lipid}} = 141$ μmol (g DCM)$^{-1}$ phospholipids in the inner and outer membranes (3, 5). With $\nu_{\text{lipid}}\, \rho_{\text{lipid}} = 55$ (32, 33), we thus obtain $f_{\text{lipid}}\rho_{\text{lipid}} = 0.045$, or 3.0% of $\rho(\omega_0^*)$. The relatively large value of $\nu_{\text{lipid}}\rho_{\text{lipid}}$ is a consequence of water penetration between the lipid headgroups, where a small number (≤4 per phospholipid) of water molecules are strongly perturbed with correlation times of order 100 ps.

In summary, we estimate that the combined contributions to $\rho(\omega_0^*)$ from phospholipids, saccharides and small molecules and ions is 5.5% for *E. coli* and 8.5% for *H. marismortui* (assuming that only the Na^+/K^+ contribution differs from *E. coli*).

Solvent-Accessible Area of Proteins and Nucleic Acids in *E. coli*. To obtain the hydration DPF ξ_{hyd}, we need to know the fraction f_{hyd} of all water in the sample that is in contact with the surfaces of proteins and nucleic acids. This fraction is estimated from the sum of the solvent-accessible areas of proteins and nucleic acids, which occur in five principal locations in an *E. coli* cell: nucleoid, ribosomes, inner and outer membranes, cytoplasm and periplasm, and external organelles (flagellae and fimbriae). We estimate the *specific* solvent-accessible surface area (SASA), a_P, of a protein or protein complex with molar mass M_P from the scaling relation

$$a_P/m^2g^{-1} = \frac{N_A 7.43 \times 10^{-18}(M_P/\text{kDa})^{0.81}}{10^3(M_P/\text{kDa})} = \frac{4474}{(M_P/\text{kDa})^{0.19}} \quad [16]$$

based on a fit (34) to calculated areas for a large set of proteins (35).

The nucleoid, which occupies a sizeable fraction of the cytoplasmic region, contains DNA, nascent *m*RNA chains and >240 protein species (36). The DNA is compacted by interactions with histone-like and other structural proteins. The nucleoid is further compacted in stationary phase (when fewer proteins are expressed). Presumably, the total SASA of the DNA is negligibly small (compared to that contributed by all proteins in the cell). The nucleoid contains two classes of proteins: permanent structural proteins and transient regulatory proteins (RNA polymerase, transcription factors). The amount and composition of the structural proteins varies strongly with growth phase, being ≈ 10 mg (g DCM)$^{-1}$ in stationary phase (37). In exponential phase (with a generation time of 50 min, as in our culture), RNA polymerase (core tetramer) accounts for 1.2% of cell protein, or 7 mg (g DCM)$^{-1}$. We shall assume that the nucleoid contains 25 mg protein (g DCM)$^{-1}$. The fundamental structural unit of the stationary-phase nucleoid is a 80 nm diameter bead, which forms fibers that loop and supercoil in the tightly packed nucleoid (38). A sphere of radius 400 Å and specific volume 0.73 ml g^{-1} has a molar mass of 221 MDa. The specific SASA is then 432 m^2 g^{-1} according to Eq. **16**. The SASA contributed by the nucleoid is then merely 11 m^2 (g DCM)$^{-1}$.

The 70S *E. coli* ribosome contains 3 RNA molecules (5S, 16S and 23S) with 4566 nucleotides and a combined molar mass of 1484 kg mol^{-1} (3, 39). With 134 mg (g DCM)$^{-1}$ rRNA (3, 5), we obtain for the amount of ribosomes n_{ribo} = 90 nmol (g DCM)$^{-1}$. The total RNA mass is reduced by 20–40% during the first several hours of starvation (40), so we shall use n_{ribo} = 63 nmol (g DCM)$^{-1}$. The solvent-accessible surface area of the ribosome (without bound *m*RNA or *t*RNA) was computed to 9346 nm^2 using the crystal structure of the intact *E. coli* 70S ribosome (41) and subtracting 2 × 85 nm^2 for the subunit interface (42). The SASA contributed by ribosomes is then 355 m^2 (g DCM)$^{-1}$.

The 30 mg (g DCM)$^{-1}$ transfer and messenger RNA (3, 5) corresponds to n_{mt} = 92 μmol nucleotide (g DCM)$^{-1}$. Using $\nu_{\text{mt}}\rho_{\text{mt}}$ = 44 (per nucleotide), as determined for a *B*-DNA dodecamer (22), we obtain from Eq. **15** $f_{\text{mt}}\rho_{\text{mt}}$ = 0.023, or 1.6% of $\rho(\omega_0^*)$. We neglect this contribution.

The ribosome contains 56 protein molecules with 7,285 residues and a combined molar mass of 805 kg mol^{-1} (39). The molar mass of the ribosome (excluding Mg^{2+} ions and other cofactors) is thus 1,484 + 805 = 2,289 kg mol^{-1}, out of which 35.2% is protein and 64.8% rRNA. We thus have 0.70 × 134 × (0.352/0.648) = 51 mg (g DCM)$^{-1}$ ribosomal protein. This is 8.9% of all protein. The surface area contribution of these proteins has already been calculated, but we must keep track of the protein mass to know how much protein is located elsewhere.

The major protein components of the outer membrane are porins (≈38 kDa, 2 × 10^5 molecules cell^{-1}) and murein lipoprotein (7.2 kDa, 7 × 10^5 molecules cell^{-1}) (9). With a total dry cell mass of 0.346 pg cell^{-1} (5), this corresponds to 36 mg (g DCM)$^{-1}$ porins and 24 mg (g DCM)$^{-1}$ mg lipoprotein. For these outer membrane proteins, Eq. **16** yields a_P = 2,242 m^2 g^{-1} (porins) and 3,075 m^2 g^{-1} (lipoprotein). Assuming that half of this area is buried in the membrane or in macromolecular contact interfaces, we find that the outer membrane proteins contribute a surface area of 77 m^2 (g DCM)$^{-1}$.

The inner (cytoplasmic) membrane contains 6–9% of the total protein mass (43), 572 mg (g DCM)$^{-1}$ (5). We use a value of 7.5%, corresponding to 43 mg (g DCM)$^{-1}$. Most of these proteins are large and we use a representative molar mass of 40 kDa, so Eq. **16** yields a_P = 2220 m^2 g^{-1}. Again, we assume that half of the surface area is buried in the membrane or in protein complexes. We thus obtain 48 m^2 (g DCM)$^{-1}$ for the surface area contributed by inner membrane proteins.

After subtraction of the nucleoid, ribosome and membrane proteins from the total protein content of *E. coli*, there remains 393 mg (g DCM)$^{-1}$ proteins located in the cytoplasm and periplasm (outside nucleoid and ribosomes) and in the external flagellae and fimbriae. The *E. coli* K-12 genome codes for 4202 proteins, ranging from 14 to 2,358 residues and with an average size of 318 ± 213 residues (www.ebi.ac.uk/integr8). We assume that the expressed proteins have a similar length distribution. Moreover, we replace the distribution by the average, using a molar mass of 318 × 109 = 35 kDa for all proteins. For this molar mass, Eq. **16** yields a_P = 2,277 m^2 g^{-1}. A substantial fraction of these proteins are associated, e.g., in enzyme complexes, cytoskeleton and external organelles. Assuming that 25% of the surface area of this protein class is buried and inaccessible to water, we obtain a solvent-accessible surface area of 671 m^2 (g DCM)$^{-1}$.

Low-Frequency Relaxation Dispersion. The dramatic increase in $R_1(\omega_0)$ at low frequencies (Fig. 1) is produced by exchange-mediated orientational randomization (EMOR) of the nuclear quadrupole coupling when internal water molecules escape from cavities within rotationally immobilized (or very large, and therefore slowly tumbling) proteins and supramolecular assemblies into the surrounding solvent, where they reorient on a picosecond time scale (23, 44–46). To simplify the analysis, we focus on the relaxation enhancement $\Delta R_1(\omega_0) \equiv R_1(\omega_0) - R_1(\omega_0^{\#})$ below a cutoff frequency $(\omega_0^{\#})/(2\pi)$ = 1 MHz. In this frequency range, the EMOR mechanism dominates strongly over protein-tumbling mediated orientational randomization, and the exchanging water molecules that induce relaxation are truly buried, rather than partially secluded in surface pockets (27). Relaxation by the EMOR mechanism can be treated rigorously even outside the (motional narrowing) regime of the conventional perturbation theory of spin relaxation (25), with the result (23, 44–46)

$$\Delta R_1(\omega_0) = \frac{\omega_Q^2}{5N_W}\sum_{k=1}^{N_{\text{int}}} S_k^2\tau_k \times \left[\frac{1}{1+(\Omega_k^2+\omega_0^2)\tau_k^2} + \frac{4}{1+(\Omega_k^2+4\omega_0^2)\tau_k^2}\right] \quad [17]$$

where the sum runs over all N_{int} internal water molecules with mean residence times τ_k (in the approximate range 0.1–10 μs) and with orientational order parameters S_k. Furthermore, $\Omega_k = (3/2)^{1/2} S_k \omega_Q$. Since the distribution of τ_k and S_k values among the internal water population is unknown, we cannot fit this expression to the data without further assumptions. Such assumptions can be avoided if we restrict our attention to the integral of the dispersion profile (47):

$$I(\omega_0^{\#}) \equiv \frac{1}{\omega_0^{\#}}\int_0^{\omega_0^{\#}} d\omega_0\, \Delta R_1(\omega_0) \quad [18]$$

To determine this integral as accurately as possible, we use a continuous interpolation function that represents the data to an accuracy commensurate with the measurement error. The natural choice is a sum of Lorentzian functions plus a constant (47)

$$R_1(\omega_0) = \alpha + \sum_{i=1}^{N_{\text{Lor}}} \beta_i \frac{1}{5}\left[\frac{\tau_i}{1+(\omega_0\tau_i)^2} + \frac{4\tau_i}{1+(2\omega_0\tau_i)^2}\right] \quad [19]$$

Unlike the residence times τ_k in Eq. **23**, the effective correlation times τ_i in Eq. **19** do not necessarily have a simple physical interpretation. They are merely parameters in a mathematical representation of the data. The number N_{Lor} of Lorentzians to be included was determined by means of the F-test with cutoff probability $P_0 = 0.90$ (47). In this way, the integral, $I(\omega_0^{\#})$, was found to converge after $N_{\mathrm{Lor}} = 6$ (*E. coli*) or 5 (*H. marismortui*) terms (Table S1). The fits were made with the Levenberg-Marquardt nonlinear least-squares algorithm with equal weighting of all data points.

Once the multi-Lorentzian representation of the MRD data has been obtained, the integral in Eq. **18** can be performed analytically as

$$I(\omega_0^{\#}) = \alpha - R_1(\omega_0^{\#}) + \frac{1}{5\,\omega_0^{\#}} \sum_{i=1}^{N_{\mathrm{Lor}}} \beta_i[\arctan(\omega_0^{\#}\tau_i) + 2\arctan(2\,\omega_0^{\#}\tau_i)] \quad [20]$$

The $I(\omega_0^{\#})$ values obtained for the two samples are given in Table 1. The uncertainty in $I(\omega_0^{\#})$ quoted in Table 1 corresponds to two standard deviations and was obtained by the Monte Carlo method with 1,000 synthetic datasets.

Combination of Eqs. **17** and **18** yields after integration

$$I(\omega_0^{\#}) = \frac{\omega_{\mathrm{Q}}^2\, n_{\mathrm{int}} S_{\mathrm{int}}^2}{5\,\omega_0^{\#}\, n_{\mathrm{W}}} \langle H_{\mathrm{cut}} \rangle \quad [21]$$

where S_{int} is the root-mean-square order parameter $\langle S_k^2 \rangle^{1/2}$, assumed to be uncorrelated with τ_k, and we have defined a dynamic cutoff function

$$H_{\mathrm{cut}}(\tau_k) \equiv \frac{\arctan(\Gamma_k) + 2\arctan(2\Gamma_k)}{[1 + (\Omega_k\tau_k)^2]^{1/2}} \quad [22]$$

$$\Gamma_k \equiv \frac{\omega_0^{\#}\tau_k}{[1 + (\Omega_k\tau_k)^2]^{1/2}} \quad [23]$$

The cutoff factor $\langle H_{\mathrm{cut}} \rangle$ in Eq. **21** is the average of $H_{\mathrm{cut}}(\tau_k)$ for the N_{int} internal water molecules.

The variation of $H_{\mathrm{cut}}(\tau_k)$ with τ_k for different values of the order parameter S_{int} is shown in Fig. S2. The maximum occurs for residence times near the quadrupole frequency ω_{Q}. If most internal water molecules have residence times shorter than the τ_k value corresponding to the maximum in $H_{\mathrm{cut}}(\tau_k)$, then the integral $I(\omega_0^{\#})$ should increase with decreasing temperature. This follows because the residence time τ_k increases strongly with decreasing temperature (48) and the other factors that enter into Eq. **21** are essentially independent of temperature (provided that the composition and internal structure of the cell do not change much). For practical reasons, this test was performed with ^{1}H MRD on H_2O-based samples. As seen from Fig. 2, $I(\omega_0^{\#})$ does, indeed, increase with decreasing temperature. A quantitative analysis according to Eq. **20** with $N_{\mathrm{Lor}} = 3$ and $\omega_0^{\#}/(2\pi) = 1$ MHz shows that $I(\omega_0^{\#})$ is 24% larger at 12°C than at 27°C. (A further increase of $I(\omega_0^{\#})$ is observed at –5°C; data not shown.) To quantify this finding, we include in Fig. S2 the analogous cutoff function for ^{1}H MRD profiles, computed with the ^{1}H EMOR theory (49). Because the effective ^{1}H–^{1}H magnetic dipole frequency ($2.36 \times 10^5\ \mathrm{s}^{-1}$ for the intramolecular coupling in H_2O) is smaller than the ^{2}H quadrupole frequency ω_{Q}, the maximum in $H_{\mathrm{cut}}(\tau_k)$ occurs at longer residence times. From the observed temperature dependence of $I(\omega_0^{\#})$, we can thus conclude that most of the internal water molecules in *E. coli* have residence times shorter than 1 μs at 27°C. The cutoff factor $\langle H_{\mathrm{cut}} \rangle$ to be used in Eq. **21** can therefore be rather precisely estimated as an average of $H_{\mathrm{cut}}(\tau_k)$ (the solid curve in Fig. S2) over the τ_k range 0.16 − 1 μs. We thus arrive at the value $\langle H_{\mathrm{cut}} \rangle = 3.4 \pm 0.3$ used to calculate $n_{\mathrm{int}} S_{\mathrm{int}}^2$ (Table 1) from Eq. **21**.

1. Tehei M, *et al.* (2007) Neutron scattering reveals extremely slow cell water in a Dead Sea organism. *Proc Natl Acad Sci USA* 104:766–771.
2. Cayley S, Lewis BA, Guttman HJ, Record MT (1991) Characterization of the cytoplasm of Escherichia coli K-12 as a function of external osmolality. *J Mol Biol* 222:281–300.
3. Neidhardt FC, Umbarger HE (1996) in *Escherichia coli and Salmonella Cellular and Molecular Biology*, ed Neidhardt FC (ASM Press, Washington, DC), Ch 3.
4. Ginzburg M, Sachs L, Ginzburg B-Z (1970) Ion metabolism in Halobacterium. *J Gen Physiol* 55:187–207.
5. Bremer H, Dennis PP (1996) in *Escherichia coli and Salmonella Cellular and Molecular Biology*, ed Neidhardt FC (ASM Press, Washington, DC), Ch 97.
6. Huisman GW, Siegele DA, Zambrano MM, Kolter R (1996) in *Escherichia coli and Salmonella Cellular and Molecular Biology*, ed Neidhardt FC (ASM Press, Washington, DC), Ch 106.
7. Mandelstam J (1958) Turnover of protein in growing and non-growing populations of Escherichia coli. *Biochem J* 69:110–119.
8. Reitzer LJ (1996) in *Escherichia coli and Salmonella Cellular and Molecular Biology*, ed Neidhardt FC (ASM Press, Washington, DC), Ch 24.
9. Nikkaido H (1996) in *Escherichia coli and Salmonella Cellular and Molecular Biology*, ed Neidhardt FC (ASM Press, Washington, DC), Ch 5.
10. Finkelstein A (1987) *Water Movement Through Lipid Bilayers, Pores, and Plasma Membranes* (Wiley, New York).
11. Gonen T, Walz T (2006) The structure of aquaporins. *Q Rev Biophys* 39:361–396.
12. Pohl P, Saparov SM, Borgnia MJ, Agre P (2001) Highly selective water channel activity measured by voltage clamp: Analysis of planar lipid bilayers reconstituted with purified AqpZ. *Proc Natl Acad Sci USA* 98:9624–9629.
13. Mallo RC, Ashby MT (2006) AqpZ-mediated water permeability in Escherichia coli measured by stopped-flow spectroscopy. *J Bacteriol* 188:820–822.
14. Navon G, Ogawa S, Shulman RG, Yamane T (1977) High-resolution ^{31}P nuclear magnetic resonance studies of metabolism in aerobic Escherichia coli cells. *Proc Natl Acad Sci USA* 74:888–891.
15. Slonczewski JL, Rosen BP, Alger JR, Macnab RM (1981) pH homeostasis in Escherichia coli: Measurement by ^{31}P nuclear magnetic resonance of methylphosphonate and phosphate. *Proc Natl Acad Sci USA* 78:6271–6275.
16. Axe DD, Bailey JE (1987) Application of ^{31}P nuclear magnetic resonance spectroscopy to investigate plasmid effects on Escherichia coli metabolism. *Biotechnol Lett* 9:83–88.
17. Eigen M (1964) Proton transfer, acid-base catalysis, and enzymatic hydrolysis *Angew Chem Int Ed* 3:1–71.
18. Liepinsh E, Otting G (1996) Proton exchange rates from amino acid side chains. Implications for image contrast. *Magn Reson Med* 35:30–42.
19. Denisov VP, Halle B (1995) Hydrogen exchange and protein hydration: The deuteron spin relaxation dispersions of bovine pancreatic trypsin inhibitor and ubiquitin. *J Mol Biol* 245:698–709.
20. Denisov VP, Halle B (2002) Hydrogen exchange rates in proteins from water ^{1}H transverse magnetic relaxation. *J Am Chem Soc* 124:10264–10265.
21. Guéron M, Leroy J-L (1995) Studies of base pair kinetics by NMR measurement of proton exchange. *Methods Enzymol* 261:383–413.
22. Denisov VP, Carlström G, Venu K, Halle B (1997) Kinetics of DNA hydration. *J Mol Biol* 268:118–136.
23. Vaca Chávez F, Hellstrand E, Halle B (2006) Hydrogen exchange and hydration dynamics in gelatin gels. *J Phys Chem B* 110:21551–21559.
24. Noguchi Y, *et al.* (2004) The energetic conversion competence of Escherichia coli during aerobic respiration studied by ^{31}P NMR using a circulating fermentation system. *J Biochem* 136:509–515.
25. Abragam A (1961) *The Principles of Nuclear Magnetism* (Clarendon Press, Oxford, UK).
26. Halle B, Denisov VP, Venu K (1999) in *Biological Magnetic Resonance*, eds Krishna NR, Berliner LJ (Kluwer Academic/Plenum, New York), pp 419–484.
27. Halle B (2004) Protein hydration dynamics in solution: a critical survey. *Philos Trans R Soc Lond Ser B* 359:1207–1224.
28. van der Maarel JRC, Lankhorst D, de Bleijser J, Leyte JC (1986) Water dynamics in aqueous electrolyte solutions from proton, deuterium, and oxygen-17 nuclear magnetic relaxation. *J Phys Chem* 90:1470–1478.
29. McLaggan D, Naprstek J, Buurman ET, Epstein W (1994) Interdependence of K^+ and glutamate accumulation during osmotic adaptation of Escherichia coli. *J Biol Chem* 269:1911–1917.
30. Ishimura M, Uedaira H (1990) Natural-abundance oxygen-17 magnetic relaxation in aqueous solutions of apolar amino acids and glycine peptides. *Bull Chem Soc Jpn* 63:1–5.
31. Uedaira H, Ikura M, Uedaira H (1989) Natural-abundance oxygen-17 magnetic relaxation in aqueous solutions of carbohydrates. *Bull Chem Soc Jpn* 62:1–4.
32. Borle F, Seelig J (1983) Hydration of Escherichia coli lipids. Deuterium T_1 relaxation time studies of phosphatidylglycerol, phosphatidylethanolamine and phosphatidylcholine. *Biochim Biophys Acta* 735:131–136.
33. Volke F, Eisenblätter S, Galle J, Klose G (1994) Dynamic properties of water at phosphatidylcholine lipid-bilayer surfaces as seen by deuterium and pulsed field gradient proton NMR. *Chem Phys Lipids* 70:121–131.

34. Halle B, Davidovic M (2003) Biomolecular hydration: From water dynamics to hydrodynamics. *Proc Natl Acad Sci USA* 100:12135–12140.
35. Liang J, Edelsbrunner H, Fu P, Sudhakar PV, Subramaniam S (1998) Analytical shape computation of macromolecules: I. Molecular area and volume through alpha shape. *Proteins* 33:1–17.
36. Pettijohn DE (1996) in *Escherichia coli and Salmonella Cellular and Molecular Biology*, ed Neidhardt FC (ASM Press, Washington, DC), Ch 98.
37. Azam TA, Iwata A, Nishimura A, Ueda S, Ishihama A (1999) Growth phase-dependent variation in protein composition of the Escherichia coli nucleoid. *J Bacteriol* 181:6361–6370.
38. Kim J, Yoshimura SH, Hizume K, Ohniwa RL, Ishihama A, Takeyasu K (2004) Fundamental structural units of the Escherichia coli nucleoid revealed by atomic force microscopy. *Nucleic Acids Res* 32:1982–1992.
39. Noller HF, Nomura M (1996) in *Escherichia coli and Salmonella Cellular and Molecular Biology*, ed Neidhardt FC (ASM Press, Washington, DC), Ch 13.
40. Siegele DA, Kolter R (1992) Life after log. *J Bacteriol* 174:345–348.
41. Schuwirth BS, *et al*. (2005) Structures of the bacterial ribosome at 3.5 Å resolution. *Science* 310:827–834.
42. Fraternali F, Cavallo L (2002) Parameter optimized surfaces (POPS): analysis of key interactions and conformational changes in the ribosome. *Nucleic Acids Res* 30:2950–2960.
43. Kadner RJ (1996) in *Escherichia coli and Salmonella Cellular and Molecular Biology*, ed Neidhardt FC (ASM Press, Washington, DC), Ch 7.
44. Halle B (1996) Spin dynamics of exchanging quadrupolar nuclei in locally anisotropic systems. *Prog NMR Spectrosc* 28:137–159.
45. Vaca Chávez F, Persson E, Halle B (2006) Internal water molecules and magnetic relaxation in agarose gels. *J Am Chem Soc* 128:4902–4910.
46. Persson E, Halle B (2008) Nanosecond to microsecond protein dynamics probed by magnetic relaxation dispersion of buried water molecules. *J Am Chem Soc* 130:1774–1787.
47. Halle B, Jóhannesson H, Venu K (1998) Model-free analysis of stretched relaxation dispersions. *J Magn Reson* 135:1–13.
48. Denisov VP, Peters J, Hörlein HD, Halle B (1996) Using buried water molecules to explore the energy landscape of proteins. *Nat Struct Biol* 3:505–509.
49. Vaca Chávez F, Halle B (2006) Molecular basis of water proton relaxation in gels and tissue. *Magn Reson Med* 56:73–81.

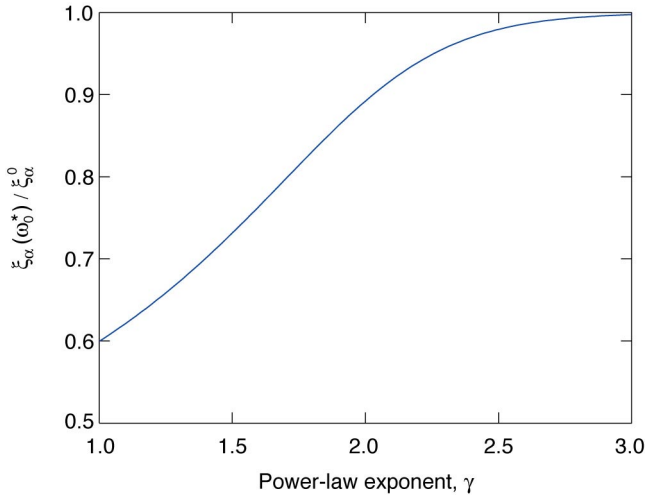

Fig. S1. Ratio of apparent to true dynamic perturbation factors for $\tau_0 = 2.8$ ps, $\tau^* = 1/\omega_0^*$ and $\omega_0^*/(2\pi) = 76.8$ MHz versus the exponent, γ, in the power-law correlation time distribution.

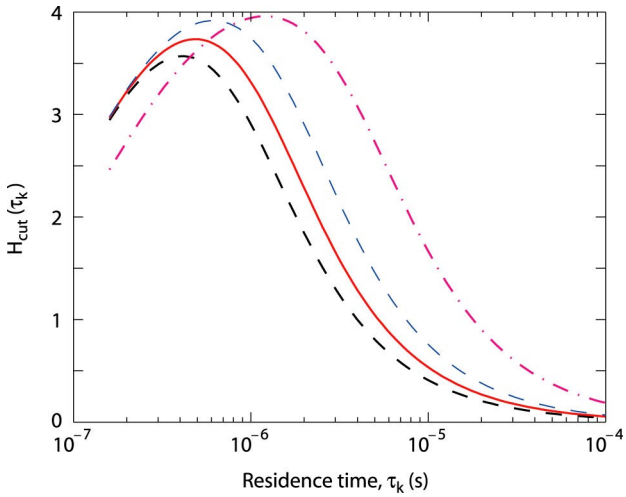

Fig. S2. Cutoff function H_{cut} versus internal water residence time τ_k for ^{1}H (magenta dash-dotted curve) and ^{2}H (the other three curves). The squared order parameter S^2_{int} was set to the most plausible value 0.6 (red solid curve and magenta dash-dotted curve) or to 0.3 (black lower dashed curve) or 1.0 (blue upper dashed curve). The latter two curves show that H_{cut} is relatively insensitive to the order parameter.

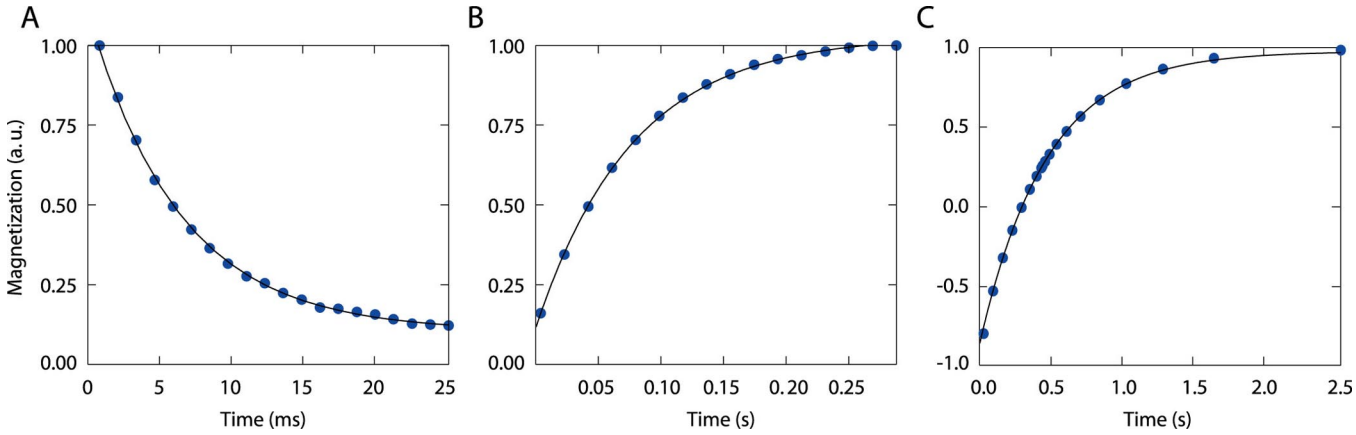

Fig. S3. Typical ^{2}H magnetization recoveries/decays measured at 1.3 kHz (*A*), 6.4 MHz (*B*), and 76.8 MHz (*C*) for the *E. coli* sample at 27°C. The curves were obtained from single-exponential three-parameter fits.

Table S1. Convergence of model-free analysis of *E. coli* MRD profile

N_{Lor}	$P(n)$	χ^2_{red}	$I(\omega_0^{\#})/s^{-1}$
1	1	798	39.8
2	1	80	25.3
3	1	6.9	26.8
4	1	2.1	26.2
5	0.90	1.4	26.7
6	0.96	0.75	26.5

Table S2. Elemental composition of *E. coli* and *H. marismortui* samples

	Mass fraction [μg (g DCM)$^{-1}$]	
Element	*E. coli*	*H. marismortui*
Al	<30	<30
As	<10	<10
Ba	1.34	0.527
Ca	434	635
Cd	<3	<2
Co	<3	<2
Cr	<3	<2
Cu	9.52	14.0
Fe	164	666
K	24,200	122,000
Mg	3,220	11,900
Mn	13.8	52.9
Mo	<3	2.67
Na	8,620	75,500
Ni	<3	<2
P	33,400	9,700
Pb	<10	<10
Si	156	46.8
Ti	3.23	2.57
V	<3	2
Zn	69.5	102
N	139,500	96,690